Journal of Power Sources 269 (2014) 898–911

Contents lists available at ScienceDirect

Journal of Power Sources

journal homepage: www.elsevier.com/locate/jpowsour

Enhancement of proton conductivity of chitosan membrane enabled by sulfonated graphene oxide under both hydrated and anhydrous conditions

Yahua Liu [a], Jingtao Wang [a, b, *], Haoqin Zhang [a], Chuanming Ma [a], Jindun Liu [a], Shaokui Cao [b], Xiang Zhang [a, *]

[a] School of Chemical Engineering and Energy, Zhengzhou University, Zhengzhou 450001, PR China
[b] School of Materials Science and Engineering, Zhengzhou University, Zhengzhou 450001, PR China

HIGHLIGHTS

- Nanohybrid membranes with polymer-nanosheet (sulfonated graphene oxide) layer were fabricated.
- Inorganic nanosheets (sulfonated graphene oxide) were uniformly dispersed in CS-based membrane.
- The membranes displayed excellent thermal and mechanical stabilities.
- The membranes achieved enhanced proton conductivities under hydrated and anhydrous conditions.
- The membranes afforded acceptable PEMFC performances under anhydrous condition.

GRAPHICAL ABSTRACT

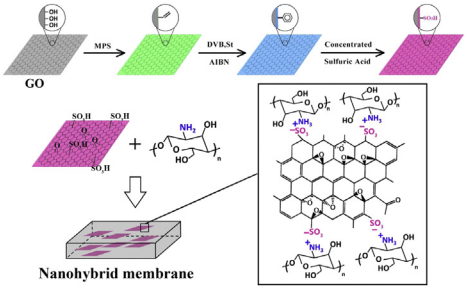

ARTICLE INFO

Article history:
Received 15 May 2014
Received in revised form
12 July 2014
Accepted 12 July 2014
Available online 19 July 2014

Keywords:
Sulfonated graphene oxide
Chitosan
Nanohybrid membrane
Acid–base pair
Proton conductivity
Fuel cell performance

ABSTRACT

In this study, sulfonated graphene oxide (SGO) nanosheets with controllable sulfonic acid group loading are synthesized via the facile distillation–precipitation polymerization, and then incorporated into chitosan (CS) matrix to prepare nanohybrid membranes. The microstructure and physicochemical properties of the resulting membranes are extensively investigated. Compared with CS control and GO-filled membranes, SGO-filled membranes attain enhanced thermal and mechanical stabilities due to the strong electrostatic attractions between $-SO_3H$ of SGO and $-NH_2$ of CS, which inhibit the mobility of CS chains. Additionally, the inhibited mobility reduces the area swellings of SGO-filled membranes, reinforcing their structural stabilities. The incorporation of SGO generates acid–base pairs along CS–SGO interface, which work as facile proton-hoping sites and thus construct continuous and wide proton transfer pathways, yielding enhanced proton conductivities under both hydrated and anhydrous conditions. Meanwhile, the conductivity can be elevated by increasing the sulfonic acid group loading and content of SGO. Particularly, incorporating 2.0% S4GO can afford the nanohybrid membrane a 122.5% increase in hydrated conductivity and a 90.7% increase in anhydrous conductivity when compared with CS control membrane. The superior conduction properties then offered a significant enhancement in H_2/O_2 cell performances to the nanohybrid membranes, guaranteeing them to be promising proton exchange membranes.

* Corresponding authors. School of Chemical Engineering and Energy, Zhengzhou University, Zhengzhou 450001, PR China.
E-mail addresses: jingtaowang@zzu.edu.cn (J. Wang), zhangxiang68@zzu.edu.cn (X. Zhang).

http://dx.doi.org/10.1016/j.jpowsour.2014.07.075
0378-7753/

1. Introduction

Fuel cells, which convert chemical energy directly into electrical energy, have been considered as promising energy conversion devices with great potential to alleviate the ever-growing demand for power [1,2]. Among various types of fuel cells, proton exchange membrane fuel cell (PEMFC) has received widespread interest due to the advantages of high energy density, easy fuel handling, environmental friendliness, and feasibility of mobile and transport applications [3–6]. As the indispensable component of PEMFC, proton exchange membrane (PEM) is required to efficiently transport protons, block fuels (i.e., methanol, hydrogen), and possess adequate structural stability for the practical application [7–9].

The commercial PEMs are the state-of-the-art perfluorosulfonic acid-based membranes (e.g., Nafion) in virtue of their high proton conductivity and stable physicochemical properties [3,10]. However, these membranes suffer from the drawbacks such as high cost, serious fuel crossover through the swollen ionic channels, and low proton conductivity under anhydrous condition, degrading their practical application in fuel cell [11]. Therefore, numerous studies have been conducted to develop alternative PEM with adequate properties and low cost [12–14]. Chitosan (CS, a deacetylated form of chitin), bearing amino and hydroxyl groups, is generally discarded as industrial waste around the world with low toxicity and cost [15,16]. Recently, CS has been explored to prepare PEM, considering its excellent film forming and fuel-barrier properties [17–19]. However, proton conduction ability of pristine CS (about 0.0117 S cm^{-1}) is low due to the absence of continuous transfer pathways and the weak conducting ability of base groups [20,21]. To overcome these intrinsic shortcomings, modification is indispensable for CS-based membranes [22–24]. One facile and efficient approach is to incorporate acid groups, such as $-SO_3H$, to CS membrane in virtue of the following advantages: (i) the acid groups can provide additional hoping sites for proton migration; (ii) the acid groups will link the base groups in CS to form acid–base pairs, which could transport protons via a water-free manner with low-energy barrier; (iii) the electrostatic attractions between acid–base pairs will confer enhanced thermal and mechanical stabilities by interfering with the CS chain mobility and packing. To sum up, the acid groups can be incorporated by blending acidic polymers, grafting acidic branched chains, or embedding acidic nanofillers [20–23]. Among these methods, embedding acidic nanofillers is considered as one of the most promising approaches, and the desired nanofillers should be compatible with CS matrix for homogeneous dispersion and meanwhile have high aspect ratio for long-range transfer pathway. Among spherical, tubular, and sheet nanofillers, nanosheet is the most ideal architecture, as its larger surface area and higher aspect ratio can donate more continuous pathways under the same filler content [20,25].

Recently, graphite oxide (GO) has been developed as an attractive nanofiller for PEM due to its unique graphitized plane structure, electric insulativity, and mechanical stability [26–28]. Besides, the oxygen-containing groups (carbonyl, hydroxyl, carboxyl, and epoxy groups) make GO easy to modify [29–32]. During the practical utilization, GO nanosheets have been generally sulfonated to acquire high proton conduction ability. Jiang et al. synthesized sulfonated graphene oxide (SGO) by grafting 3-mercaptopropyl trimethoxysilane to GO surface and then being oxidized by H_2O_2 [29]. Ravi et al. prepared SGO through sulfonation of GO using diazonium salt, which was prepared by adding $NaNO_2$ to the mixture of NaOH and sulfanilic acid, followed by dissolved in ice water and concentrated HCl [32]. For these methods, the sulfonic acid group loading amount is usually limited and/or the modification process is cumbersome and time-consuming.

Herein, SGO with high and controllable sulfonic acid group loading amount was synthesized via a facile distillation–precipitation polymerization for the first time. The SGO was employed to enhance the proton conductivity of CS membrane. The microstructure and physicochemical characteristics of the resulting membranes were investigated in detail. The proton conduction properties under both hydrated and anhydrous conditions were systematically evaluated. Moreover, the PEMFC performances of the membranes were explored. By doing so, it is demonstrated that the SGO gave significant enhancement in the proton conduction and cell performances to CS-based membrane, together with adequate thermal and mechanical properties.

2. Experimental

2.1. Materials and chemicals

CS with the deacetylation degree of 91% was supplied by Golden-Shell Biochemical Co. (Zhejiang, China) and used as received. Natural graphite powders (~45 μm) were purchased from Sinopharm Chemical Reagent. Styrene (St) and 3-(methacryloxy) propyltrimethoxysilan (MPS) were obtained from Aldrich and distilled under vacuum. Divinylbenzene (80% DVB isomers) was supplied as technical grade by Shengli Chemical Technical Faculty, Shandong, China, and was washed with 5% aqueous sodium hydroxide and water, then dried over anhydrous magnesium sulfate. 2,2′-Azobisisobutyronitrile (AIBN), acetonitrile, and sulfuric acid were purchased from Kewei Chemistry Co., Ltd (Tianjin, China). Deionized water was used throughout the experiment.

2.2. Synthesis of SGO

GO nanosheets were prepared by oxidizing natural graphite powders according to the improved method in literature [33]. SGO were synthesized through distillation–precipitation polymerization method [34]: GO (5.0 g) was dispersed into the mixture of ethanol (180 mL), water (20 mL), and aqueous solution of ammonium (15 mL) with vigorous stirring at 25 °C for 24 h. Then, MPS (2.0 mL) was added into the resultant mixture. After being stirred for another 24 h, the MPS-modified GO was purified by centrifugation and followed by drying in a vacuum oven. MPS-modified GO (0.30 g), St (0.50 mL), crosslinker DVB (0.50 mL), and AIBN (0.02 g) were dissolved by ultrasonic treatment in acetonitrile (80 mL) in a dried flask. The mixture was heated and kept boiling state until half acetonitrile was distilled out. Afterward, the modified GO was purified and dried for sulfonation. The resultant modified GO was sulfonated by concentrated sulfuric acid (94%) at 40 °C for 2 h or 4 h to obtain S2GO or S4GO, respectively.

2.3. Preparation of the membranes

CS (1.2 g) was dissolved in acetic acid aqueous solution (30 mL) and stirred for 2 h at room temperature. Simultaneously, a certain amount of GO or SGO was dispersed into water (30 mL) with ultrasonic treatment for 24 h. Afterward, these two solutions were mixed together and stirred vigorously for another 24 h. The resultant homogenous solution was cast onto a clear glass plate and dried at 30 °C for 72 h to obtain a nanohybrid membrane. The obtained membrane was then immersed in 1.0 M sulfuric acid solution for 24 h to completely crosslink the CS matrix, following by extensively rinsing with water to remove the residual acid. After being dried, the nanohybrid membranes were obtained and designated as CS/GO-X, CS/S2GO-X or CS/S4GO-X representing GO, S2GO or S4GO as the nanofillers, where X ($X = 0.5, 1.0, 1.5, 2.0$, and 2.5) represented the weight percentage of the nanofillers to CS. CS

control membrane was fabricated in exactly the same way as described above without incorporating any nanosheets. The average thickness of the dry membranes fell in the range of 60–68 μm.

2.4. Characterization of the GO, SGO, and membranes

Transmission electron microscopy (TEM), utilized to characterize the morphology of GO and SGO, was performed on a FEI model TECNAI G2 transmission electron microscope (acceleration voltage, 200 kV). Fourier transform infrared (FTIR) spectroscopy was recorded on a Nicolet (MAGNA-IR 560) with the wavelength range from 4000 to 400 cm^{-1} at room temperature. Thermogravimetric analysis (TGA) was conducted by TGA-50 SHIMADZU from 30 to 800 °C at 10 °C min^{-1} under N_2 atmosphere. The microstructures of the membranes were observed using scanning electron microscope (SEM, JSM 7500F) after being freeze-fractured in liquid nitrogen and then sputtered with gold. Differential scanning calorimetry (DSC, 204 F1 NETZSCH) was conducted as follows: sample was preheated from room temperature to 120 °C at the heating speed of 10 °C min^{-1}, then cooled to 80 °C and reheated to 260 °C. The mechanical properties of membranes (1.0 × 4.0 cm) were collected by an Instron mechanical tester (Testometric 350 AX) with an elongation rate of 2 mm min^{-1} at room temperature. RigakuD/max2500v/Pc X-ray diffraction (XRD, CuK 40 kV, 200 mV) was utilized to characterize the crystalline structures of the nanosheet and membranes.

2.5. Measurement of water uptake and area swelling

Water uptake was determined by measuring the change in weight between the dry and wet membrane. The membrane was first dried at 80 °C for 24 h to obtain the dry weight (W_{dry}). Afterward, the membrane was immersed in water for 48 h at 25 °C to be saturated. Finally, it was taken out and re-weighed (W_{wet}) after removing the surface liquid droplets. The value of water uptake was the average of three measurements with an error within ±4.0% and calculated by the equation (1):

$$\text{Water uptake}(\%) = \left(W_{wet} - W_{dry}\right) \Big/ W_{dry} \times 100 \quad (1)$$

Area swelling of the membrane was determined in a similar way: soaking the pre-measured membrane (A_{dry}, cm^2) in water for 48 h at 25 °C and then re-measuring the wet membrane area (A_{wet}, cm^2). Area swelling was defined as:

$$\text{Area swelling}(\%) = \left(A_{wet} - A_{dry}\right) \Big/ A_{dry} \times 100 \quad (2)$$

2.6. Evaluation of ion exchange capacity (IEC), proton conductivity, and PEMFC performance

IEC values of the nanosheets and membranes were evaluated via acid–base titration method. A dry pre-weighted membrane was immersed in the saturated 2.0 M NaCl solution for 48 h to completely liberate the H^+ into the solution by exchanging with Na^+. The solution was then titrated by 0.01 M NaOH solution using phenolphthalein as indicator at room temperature. The *IEC* value was calculated by the equation (3):

$$IEC\left(\text{mmol g}^{-1}\right) = 0.01 \times 1000 \times V_{NaOH}/W_d \quad (3)$$

where V_{NaOH} and W_d were the volume of NaOH solution used in titration and the weight of the dry membrane, respectively. The measurement of *IEC* was carried out with an accuracy of 0.001 mmol g^{-1}.

The proton conductivity measurement was conducted in a conductivity cell by AC impedance spectroscopy method. The membrane impedance was tested by a frequency response analyzer (FRA, Compactstat, Ivium Tech.) with the oscillating voltage of 20 mV over a frequency range of 10^6–10 Hz. To test the proton conductivity under hydrated condition, the sample was immersed in water for 48 h to be fully hydrated prior to the measurement. Then, the sample was put in the cell and heated by water vapor under a certain temperature ranging from 20 to 80 °C. The relative humidity (RH) was kept at 100% throughout the test. The sample was kept for a period of time until the resistance became a constant value. Proton conductivity under anhydrous condition was tested using dry air after the membrane was completely dried at 60 °C for 24 h under high vacuum. The proton conductivity (σ, S cm^{-1}) of the sample was calculated by the equation (4):

$$\sigma = l/AR \quad (4)$$

where l, A, and R were the membrane thickness, membrane area, and membrane resistance, respectively.

The single PEMFC performances of the membranes under anhydrous condition were performed according to the literature [35,36]: the membrane electrode assemblies (MEAs, 2.0 cm × 2.0 cm) were hot-pressed at 135 °C and 4.0 MPa for 2.0 min. The Pt catalyst loadings for both anode and cathode were 0.3 mg cm^{-2}. Then, the MEAs were conducted using an in–house single fuel cell test set-up, in which the MEA was sandwiched between two graphite plates with flow clusters. The single PEMFC was operated under 120 °C with dry H_2/O_2, and the flux rates of H_2 and O_2 were 150 and 200 mL min^{-1}, respectively. The single cell was first activated using hydrous H_2 (humidification temperature, 30 °C) for 4 h, and followed by keeping under the operation conditions for at least 4 h.

3. Results and discussion

3.1. Synthesis of SGO

The synthesis process of SGO could be divided into three steps as illustrated in Scheme 1: the first step was the grafting of MPS onto the surface of GO to introduce reactive vinyl groups; the second step was the formation of polymeric layer (poly(DVB-*co*-St)) through distillation–precipitation polymerization, in which St donated phenyl groups while DVB worked as crosslinker; and the third step was the sulfonation of phenyl groups to graft sulfonic acid groups within the polymeric layer. During the third step, the sulfonic acid group loading amount was tailored by the sulfonation time and two kinds of SGOs with different loading amount were obtained and designated as S2GO and S4GO.

Morphological features of GO, S2GO, and S4GO were observed in their TEM images as shown in Fig. 1. Conforming to the shape of the parent graphite, GO was exfoliated into nanosheets, which agglomerated driven by the strong interlayer attractions (Fig. 1a). Since the sulfonation reaction mainly occurred on the poly(DVB-*co*-St) layer, the morphology of the nanosheets was slightly altered after the sulfonation, and S2GO (Fig. 1b) and S4GO (Fig. 1c) remained the sheet structure. For SGO, the presence of $-SO_3H$ groups weakened the interlayer interactions, thereby preventing their stacking and reducing the contact area.

The existence of sulfonated polymeric layer on the surface of SGO was probed by FTIR, *IEC*, and TGA. The FTIR spectrum of GO in Fig. 2a showed all the characteristic bands corresponding to oxygen functional groups, including 1730 cm^{-1}(stretching vibrations

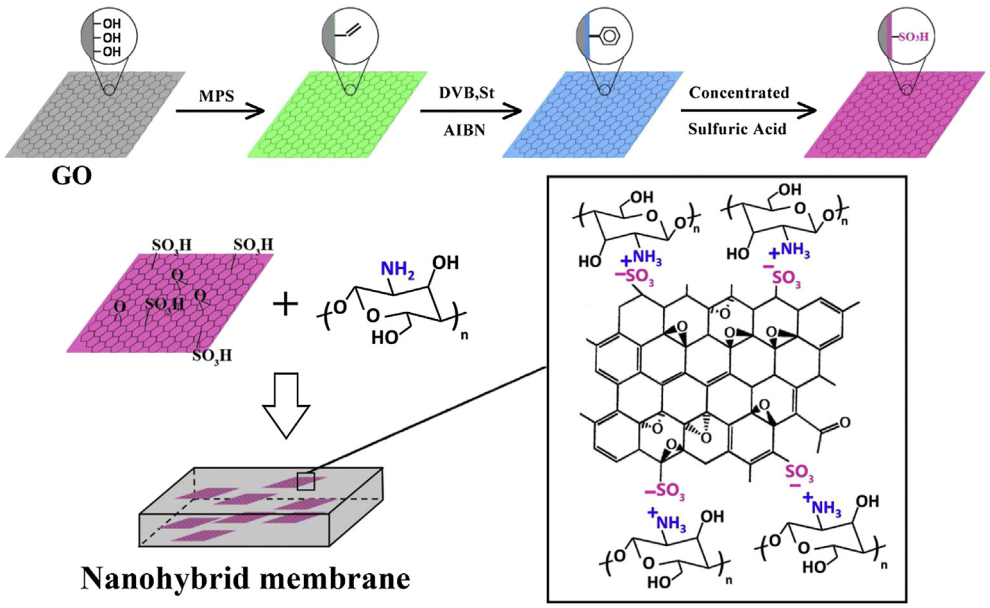

Scheme 1. Preparation of SGO and the microstructure of nanohybrid membrane.

from C=O), 1633 cm^{-1} (broad-coupling from O–H), and 1382 cm^{-1} (deformation from C–OH). During the surface modification, MPS was grafted onto the GO surface through dehydration with the C–OH groups in GO. In such a way, the characteristic band near 1382 cm^{-1} disappeared in the spectra of S2GO and S4GO. Although the major vibration bands associated with O=S=O of $-SO_3H$ (1218, 1075, and 1022 cm^{-1}) could not be discriminated since they were overlapped by the broad band of GO near 1170 cm^{-1}. Two new bands at 2924 and 2850 cm^{-1} were observed, which were assigned to the –S–OH and $-CH_2-$, respectively. Additionally, the intensities of these two bands of S4GO were stronger than those of S2GO, indicating the higher sulfonic acid group loading amount of S4GO. To quantificationally determine the loading amount of $-SO_3H$, the *IEC* values of these three kinds of nanosheets were obtained, among which the *IEC* value of GO was 1.622 mmol g^{-1} resulting from the dissociated H^+ from carboxyl groups. After sulfonation, the *IEC* values of S2GO and S4GO rose to 1.827 and 1.956 mmol g^{-1}, respectively. Notably, the acquired sulfonic acid group loading amount was much higher than the reported value in literature [37]. The *IEC* increase corroborated the successful incorporation of high conducting $-SO_3H$ into GO, and its loading amount in SGO could be facilely tuned by the sulfonation time.

TGA results in Fig. 2b revealed that GO underwent three-stage weight loss, including the evaporation of moisture (mainly bonded water) as the first stage (30–150 °C), the deoxygenation of GO (mainly oxygen-containing groups) as the second stage (180–280 °C), and the decomposition of nanosheets backbone (mainly C–C bonds) as the third stage (280–800 °C). By comparison, the sulfonated polymeric layer afforded enhanced water retention ability to SGO, providing a higher weight reduction during the first stage. Meanwhile, the higher sulfonic acid group loading amount gave S4GO higher weight reduction than that of S2GO during this stage. During the second stage, the coverage of cross-linked polymeric layer prevented the deoxygenation of SGO, and the weight reduction was therefore assigned to the pyrolysis of $-SO_3H$. Therefore, the weight loss of S2GO (10.8%) or S4GO (12.1%) was lower than that of GO (37.4%). Together with the decomposition of GO, the decomposition of polymeric layer resulted in lower char yields for S2GO (24.8%) and S4GO (20.9%) than that of GO (32.2%). In summary, these observations confirmed that the GO was successfully functionalized by the polymeric layer with $-SO_3H$ groups.

Fig. 2c showed the XRD spectra of GO, S2GO, and S4GO. Different from the diffraction peak of graphite at 27° (001), this peak shifted to 10.1° for GO because of the inserting of oxygen-containing

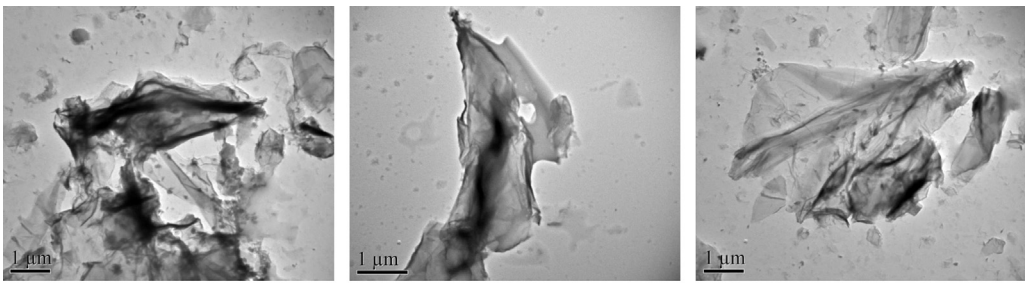

Fig. 1. TEM images of the nanosheets: (a) GO, (b) S2GO, and (c)S4GO.

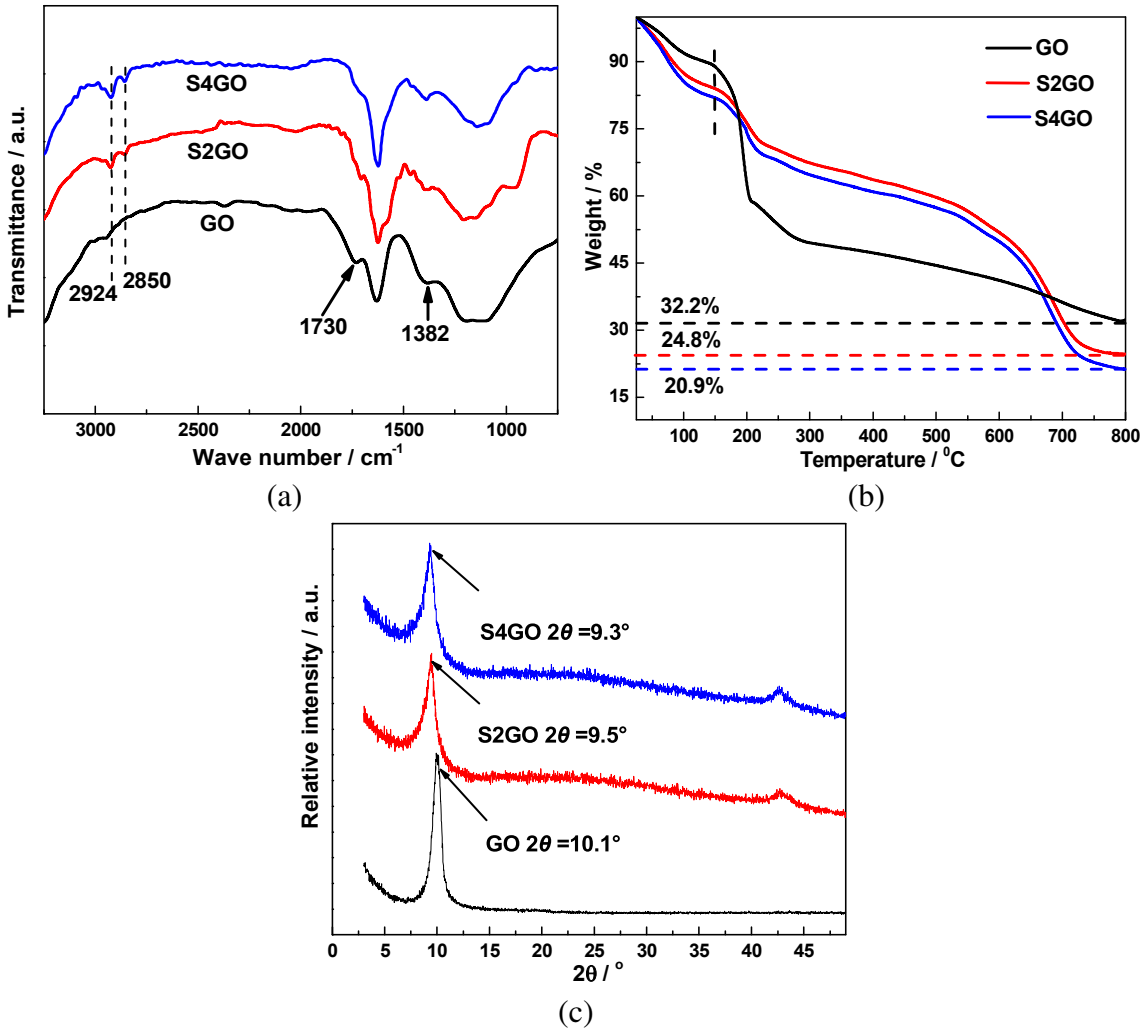

Fig. 2. (a) FTIR spectra, (b) TGA curves, and (c) XRD patterns of GO, S2GO, and S4GO.

groups, which increased the average interlayer distance from 0.34 nm to 0.89 nm. After modification, this diffraction peak decreased to 9.5° for S2GO and 9.3° for S4GO, corresponding to the interlayer distances of 0.95 and 0.97 nm, respectively. The increase of the distance should be ascribed to the entering of hydrophilic monomer molecules into GO interlayer during the modification. The close data for S2GO and S4GO suggested that they possessed similar sheet morphologies. Accordingly, the sulfonic acid group loading amount of SGO should be the main determiner of the properties and performances of S2GO-filled and S4GO-filled membranes.

3.2. Preparation of the membranes

The GO, S2GO, and S4GO were then embedded into CS matrix to prepare nanohybrid membranes via solution casting method. To better understand the interfacial interaction between nanosheets and CS, the FTIR spectra of CS, CS/GO-1.5, CS/S2GO-1.5, and CS/S4GO-1.5 were performed and shown in Fig. 3a. Three characteristic bands around 3260, 1628, and 1527 cm^{-1} were clearly observed for all the membranes, which were assigned to the characteristic bands of CS, viz., hydroxyl, amide I, and amide II groups, respectively. The band at 1151 cm^{-1} was corresponded to C—O stretching vibrations of C—OH in CS chains. The intensities of these characteristic bands in the spectra of nanohybrid membranes became weak when compared to CS control membrane, inferring the generation of interfacial attractions (e.g., hydrogen-bonding and electrostatic interactions) between the —OH/—NH_2 groups of CS and the acid groups of nanosheets. Compared with GO-filled membrane, SGO-filled membranes gave rise to a new peak at 898 cm^{-1} (dashed line), which corresponded to the symmetric stretching of —S—O^- group. This group was reasonably from the deprotonation of —SO_3H on SGO driven by the —NH_2 in CS matrix. In this manner, acid—base pairs were generated along SGO surface in the form of —$SO_3^-\cdots{}_3HN^+$— (Scheme 1). The influence of the nanosheet content on interfacial interaction was probed and the results were shown in Fig. 3b. It could be observed that the intensities of the characteristic bands of CS gradually decreased with the increase of S2GO content from 0.5% to 2.5%, which was attributed to the increase of acid—base pairs and hence the interfacial attractions.

The inner microstructures and nanosheet dispersion of nanohybrid membranes were probed using their SEM images of cross-section. Fig. 4a showed that CS control membrane was dense and smooth, without obvious cracks or pinholes. In comparison, the cross-section of the nanohybrid membranes became rougher and displayed obvious wrinkles due to the presence of nanosheets (assigned in Fig. 4b–d). Besides, the overall morphology of the

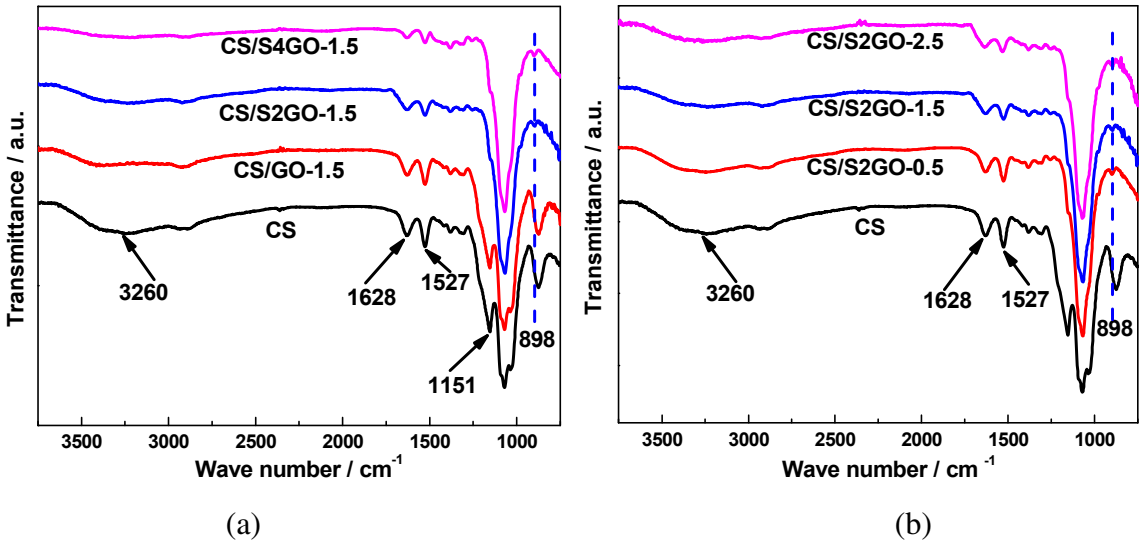

Fig. 3. FTIR spectra of CS control and nanohybrid membranes.

nanohybrid membranes was uniform without cracks. This observation suggested that the nanosheets (GO, S2GO, and S4GO) were well dispersed within CS matrix as a result of the strong interfacial interactions, making a good compatibility between CS and nanosheets. For the nanohybrid membranes, SGO-filled membranes possessed more wrinkles than GO-filled membrane, inferring much better dispersion of the SGO. The well dispersion of SGO would provide more continuous pathways for proton migration.

The crystalline structure obviously affected the transfer resistance of a membrane. XRD was utilized to investigate the

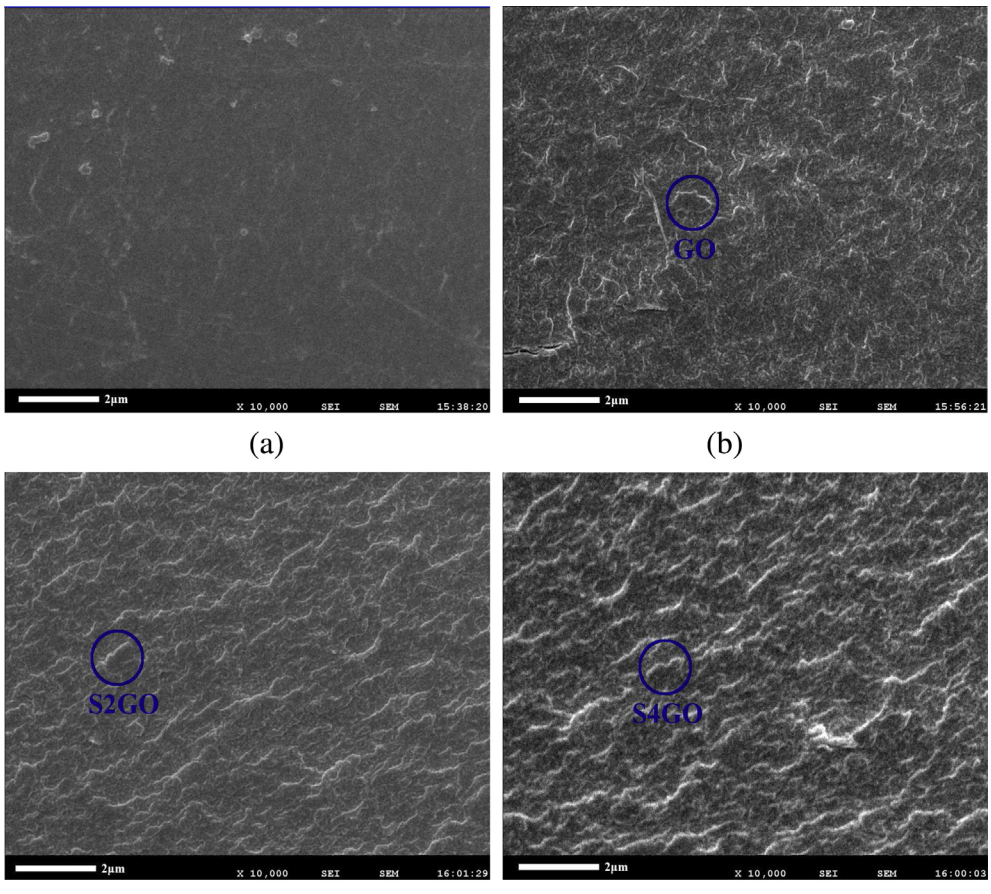

Fig. 4. SEM images of the cross-section of (a) CS, (b) CS/GO-1.5, (c) CS/S2GO-1.5, and (d) CS/S4GO-1.5.

crystalline structure of the as-prepared membranes and the patterns were depicted in Fig. 5. Similar to the results in literature, CS control membrane exhibited three characteristic bands at $2\theta = 22.6°$, 19.2°, and 11.9° [38]. By comparison, the bands for CS matrix at $2\theta = 11.9°$ and 19.2° weakened or even disappeared when adding GO/SGO nanosheets. Such observations should be ascribed to the presence of nanosheets, which interfered with the ordered packing of CS chains through the interfacial interactions and thus reduced their crystallinity domains. Fig. 5b revealed that the interference of nanosheets on the crystallinity of CS became stronger with the increase of nanosheet content, and the intensities of the characteristic bands gradually decreased.

3.3. Thermal and mechanical properties of the membranes

Excellent thermal and mechanical stabilities are required for a PEM to achieve long-term operation. TGA and DSC measurements were carried out to investigate the thermal properties of the as-prepared membranes. TGA results in Fig. 6a,b suggested that all the membranes underwent the following three-step weight loss: (i) the first stage was the evaporation of water from the membrane around 30–150 °C, (ii) the second stage was the degradation of CS side-chains around 210–310 °C, and (iii) the third stage was the degradation of CS backbones around 450–650 °C. By comparison, GO-filled membrane displayed a similar thermal degradation behavior to that of CS control membrane, inferring that the degradation mechanism of CS might remain unchanged after incorporating GO. However, the TGA curves of CS/S2GO-1.5 and CS/4GO-1.5 were retarded at the second and third stages when compared with that of CS control membrane, that is, they had higher onset temperatures at these two stages. The electrostatic interactions between CS and SGO should contribute to the increased temperatures, which delayed the degradation of CS chains by inhibiting their motion. It should be noted that the residues of SGO-filled membranes were higher than that of GO-filled membrane, which was opposite to the order of that of nanosheets (SGO < GO). Such phenomenon was reasonably ascribed to the inhibited decomposition of CS chains in CS/SGO-X. Although the residues formed by SGO were lower than that formed by GO, the incorporation of SGO would cause CS matrix in CS/SGO-X to leave more residues. Collectively, SGO-filled membrane had more residues than GO-filled membrane. Similar observation was found in other nanocomposites [38,39]. Elevating the SGO content would enhance the thermal stability of the nanohybrid membrane, as proved in Fig. 6b. TGA results implied that the as-prepared membranes were thermally stable at the temperatures below 200 °C, adequate for the application of PEMFC.

The chain mobility of the as-prepared membranes was probed by DSC and the results were shown in Fig. 6c,d. Endothermic peak at the temperatures ranging of 219–243 °C could be observed for all the membranes, which was assigned to the thermal decomposition of CS side-chains. It was found that CS control membrane displayed a transition temperature (T_d) of 219.4 °C. Incorporating the nanosheets would suppress the CS decomposition by the interfacial interactions, thus significantly increasing the T_d. For instance, CS/GO-1.5, CS/S2GO-1.5, and CS/S4GO-1.5 attained the T_d of 224.1, 232.8, and 236.5 °C, respectively. For another, increasing the nanosheet content improved the thermal stabilities of nanohybrid membranes, yielding a continuous increase of T_d from 226.7 to 242.5 °C as the S2GO content increased from 0.5 to 2.5% (Fig. 6d). In summary, DSC results indicated that the thermal stability of the membrane was effectively improved upon SGO incorporation, which was in agreement with the results of TGA.

Fig. 7 presented the stress–strain curves of the as-prepared membranes for probing their mechanical properties. CS control membrane exhibited acceptable mechanical stability with the Young's modulus of 692.3 MPa, along with the tensile strength of 44.7 MPa and the elongation at break of 17.7%. By comparison, the nanohybrid membranes acquired enhanced mechanical stabilities. For instance, incorporating 1.5% GO, S2GO, or S4GO elevated the tensile strength to 64.3, 79.8, or 85.3 MPa, along with the Young's modulus of 1614.7, 2302.4, or 2697.4 MPa, respectively. The enhanced mechanical properties were reasonably ascribed to the interfacial interactions, which inhibited the mobility of CS chains and made their stretching more laborious. The influence of nanosheet content on mechanical strength was investigated, taking CS/S2GO-X as an example. It was found that as the S2GO content increased from 0.5% to 2.5%, both the tensile strength and Young's modulus first increased and then decreased (Fig. 7b). CS/S2GO-1.5 possessed the highest modulus and strength of 2302.4 and 83.3 MPa, respectively, which dropped to 1805.9 and 77.0 MPa when the content was up to 2.5%. This reduction might be caused by the aggregation of S2GO under this high content.

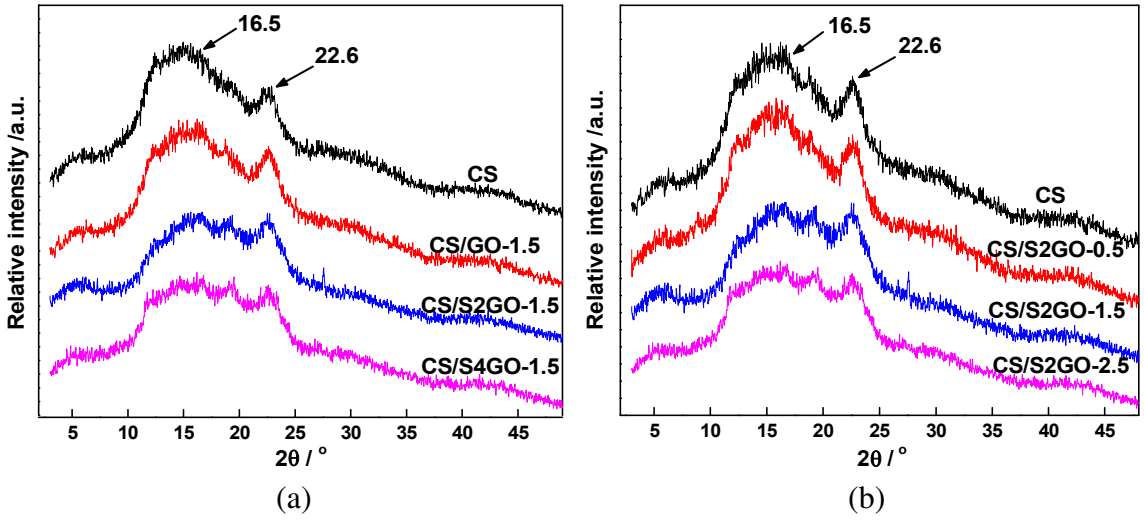

Fig. 5. XRD patterns of CS control and nanohybrid membranes.

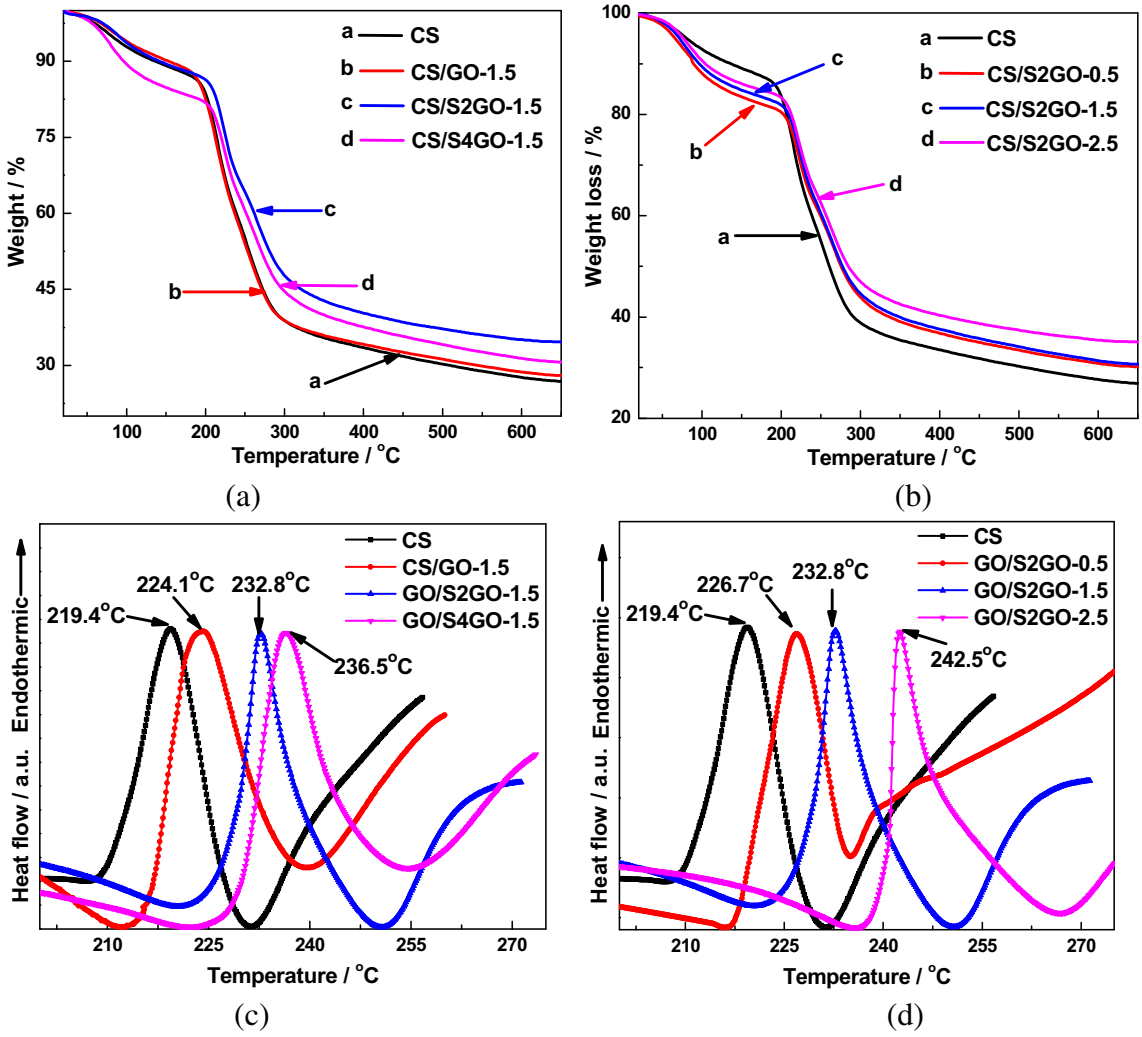

Fig. 6. TGA (a and b) and DSC (c and d) curves of CS control and nanohybrid membranes.

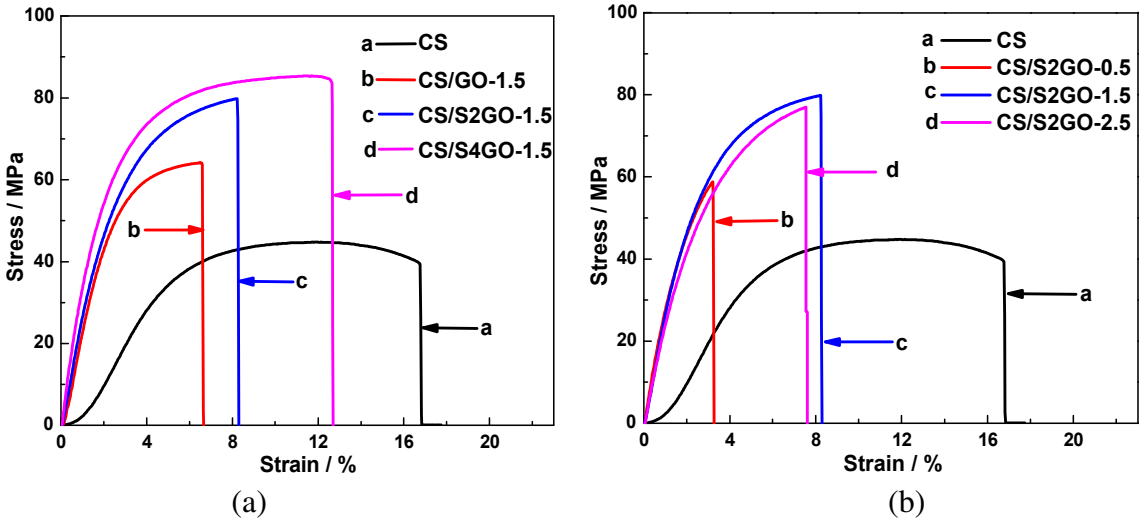

Fig. 7. Stress–strain curves of CS control and nanohybrid membranes.

3.4. Water uptake and area swelling of the membranes

Water uptake is one crucial parameter for high-performance PEM since water molecules participate in both of the proton transfer mechanisms, including vehicle mechanism and Grotthuss mechanism [40]. However, excessive water uptake will lead to severe swelling and then increase the fuel crossover and reduce the structural stability. Fig. 8a revealed that CS control membrane showed the high water uptake of 76.7% at 25 °C due to the hydrophilic groups (i.e., −OH and $-NH_2$). Incorporating the nanosheets would inhibit the chain motion and hence the free volumes of CS matrix, the main locations for water storage. Consequently, the nanohybrid membranes displayed reduced water uptakes. For instance, the uptakes of CS/GO-1.5, CS/S2GO-1.5, and CS/S4GO-1.5 were 64.9%, 61.0%, and 59.7%, respectively. For another, although SGO had higher water absorption ability than GO as testified by TGA analysis, the reduced chain motion in SGO-filled membrane would make the CS matrix store less water when compared with that in GO-filled membrane. Collectively, the SGO-filled membranes showed lower water uptakes than GO-filled membrane. Elevating the nanosheet content would decrease the water absorption ability, letting the uptake of CS/S2GO-X decrease from 70.1% to 54.2% with the S2GO content increasing from 0.5% to 2.5% as an example. Generally, the adsorption of water would cause the membrane to swell through hydration, and high water uptake usually gave a high area swelling [20]. Similar to the uptake behavior, Fig. 8b revealed that the area swelling decreased in the order of CS > CS/GO-X > CS/S2GO-X > CS/S4GO-X under identical conditions. The reduction of swelling upon SGO incorporation endowed the nanohybrid membranes with enhanced structural stabilities, making them more suitable for the practical application.

3.5. Proton conduction properties of the membranes

3.5.1. IEC of the membranes

IEC, an indication of the number of ion exchangeable groups and available protons, is an important parameter for proton conduction. *IEC* values measured by classical titration method were shown in Fig. 8c, which revealed that CS control membrane displayed a relatively low *IEC* of 0.195 mmol g^{-1}, close to the value reported in literature [41]. By comparison, the *IEC* values of GO-filled membranes were enhanced after the incorporation of GO, resulting from the available proton conducting groups (e.g., $-CO_2H$). Upon modification by the high-conducting $-SO_3H$, the nanosheets (SGO) donated higher *IEC* values to SGO-filled membranes than those of GO-filled membranes. Additionally, increasing the sulfonic acid group loading amount on SGO would elevate the proton exchange capability, providing CS/S4GO-X higher *IEC* than CS/S2GO-X. For

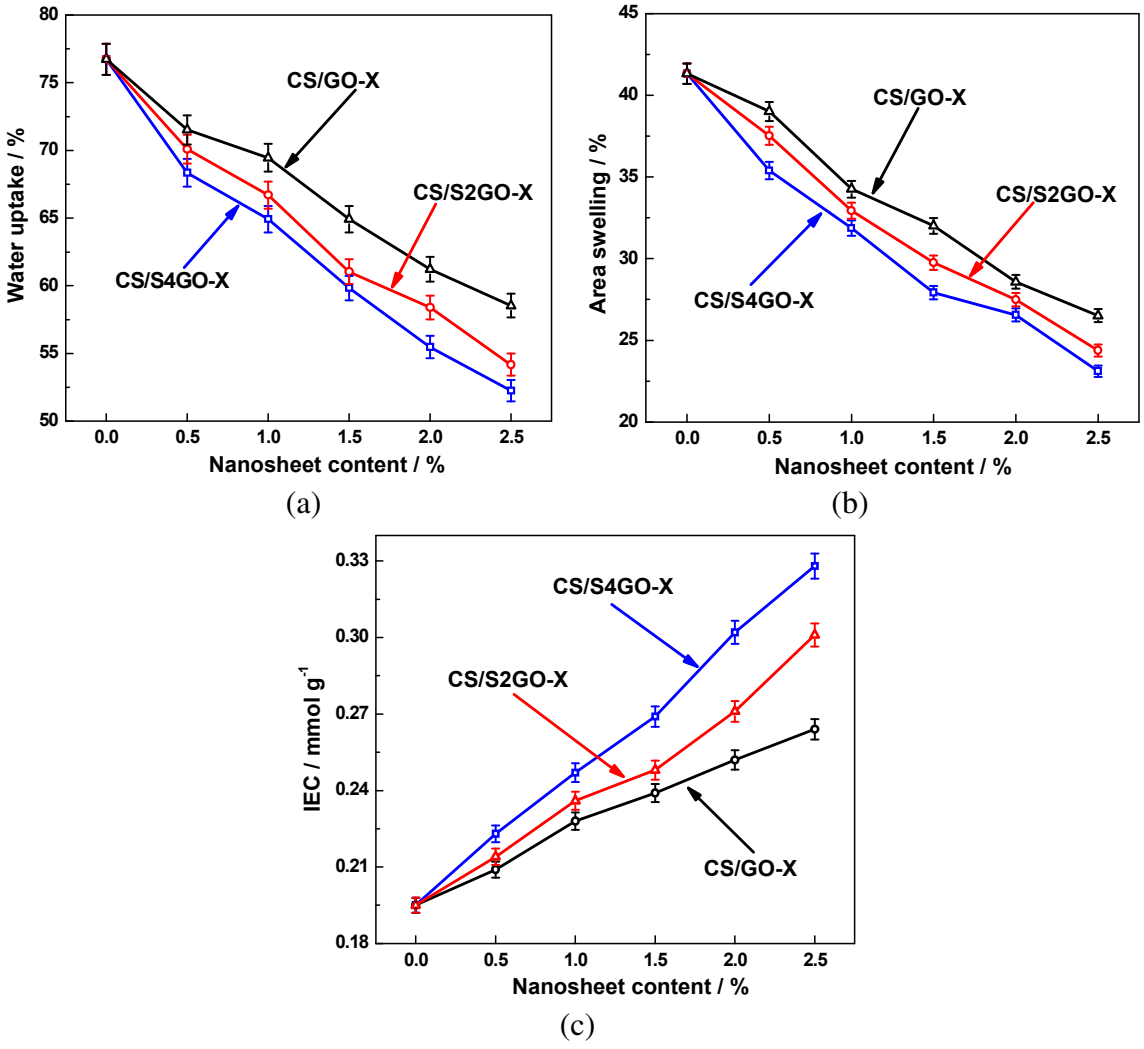

Fig. 8. (a) Water uptake, (b) area swelling, and (c) *IEC* of CS control and nanohybrid membranes at 25 °C.

instance, the *IEC* values of 0.214 and 0.223 mmol g^{-1} were acquired when 0.5% S2GO and S4GO were added, respectively. Meanwhile, the *IEC* value of nanohybrid membrane increased with the increase of the nanosheet content. Taking CS/S2GO-X as an example, increasing the S2GO content from 0.5% to 2.5% afforded an increase of *IEC* from 0.214 to 0.301 mmol g^{-1}.

3.5.2. Proton conductivity of the membranes under hydrated condition

As the key indicator of a PEM, proton conductivity is the performance-limiting parameter by determining the operational voltage and current output of a fuel cell [42]. Proton conductivities under both hydrated (100% RH) and anhydrous (0% RH) conditions were conducted for better understanding the function of SGO on proton transfer. The conductivities at 25 °C and 100% RH were shown in Fig. 9a. It was found that CS control membrane attained a conductivity of about 0.0117 S cm^{-1}, close to the result in literature [20,41]. The incorporation of SGO nanosheets significantly facilitated the proton transfer through nanohybrid membranes, yielding the conductivity of 0.0174 or 0.0182 S cm^{-1} with the enhancement of 49% or 56% when adding only 0.5% S2GO or S4GO, respectively. As mentioned in water uptake, proton transfer through a PEM obeyed the vehicle mechanism and Grotthuss mechanism. Vehicle mechanism was related to the protons diffusing in the form of H_3O^+, $H_5O_2^+$, or $H_9O_4^+$, while Grotthuss mechanism was related to the protons hoping from one carrier site to the neighboring one [43,44]. Considering the fact that SGO reduced the water uptake and area swelling of nanohybrid membranes, which in turn would reduce the vehicle-type transporting protons, the enhanced conductivities should be attributed to the increase of Grotthuss-type transporting protons. The transfer was reasonably promoted by: (i) the presence of abundant sulfonic acid groups within the membrane, which worked as additional proton-hoping sites; (ii) the generation of acid–base pairs ($-SO_3^-\cdots{}_3HN^+-$), which served as low-barrier proton-hoping sites; and (iii) the sheet structure and high specific surface area, which allowed SGO to create wide and continuous pathways using the hoping sites. Fig. 9a indicated that the proton conductivities of the nanohybrid membranes could be effectively enhanced by increasing the sulfonic acid group loading amount or content of SGO. Notably, CS/S4GO-2 achieved the highest conductivity of 0.0267 S cm^{-1}, 222.5% of that of CS control membrane. When further increasing the S4GO content to 2.5%, a reduction of conductivity was observed probably due to the nanosheet agglomeration. Under identical conditions, GO nanosheets displayed similar function in elevating the conductivity of the nanohybrid membrane through the conducting $-CO_2H$ groups.

The temperature-dependent conductivities under hydrated condition were shown in Fig. 9b–d. It was found that all the

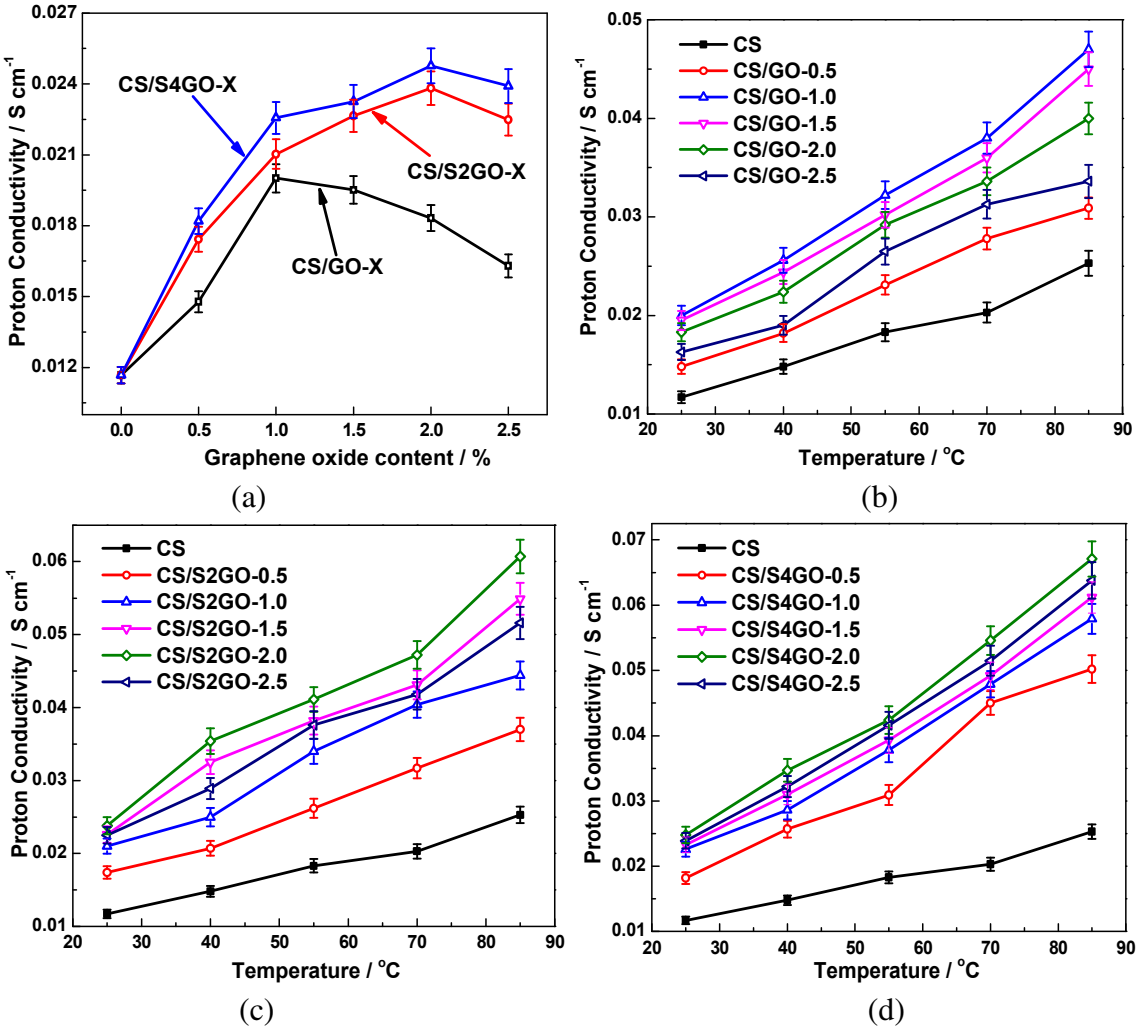

Fig. 9. (a) Proton conductivity at 25 °C under 100% RH, and temperature-dependent conductivity of (b) CS/GO-X, (c) CS/S2GO-X, and (d) CS/S4GO-X under 100% RH.

membranes exhibited gradual increase of conductivity with the temperatures varying from 25 to 85 °C, resulting from the promoted motion of polymer chains and water molecules at high temperature. For instance, the conductivity of CS control membrane increased from 0.0117 to 0.0253 S cm^{-1}. By comparison, the nanohybrid membrane possessed higher conductivity than that of CS control membrane under every testing temperature, meanwhile following the order of CS < CS/GO-X < CS/S2GO-X < CS/S4GO-X. For another, as the temperature increased from 25 to 85 °C, conductivity enhancements from 0.0195 to 0.0450, from 0.0226 to 0.0549, and from 0.0233 to 0.0612 S cm^{-1} were obtained for CS/GO-1.5, CS/S2GO-1.5, and CS/S4GO-1.5, with the growth rate of 130.7%, 142.9%, and 162.6%, respectively. Such results inferred that the transfer ability of acid–base pairs could be elevated by increasing the temperature, as the activated motion of acid–base pairs made the enthalpy change smaller during proton hoping at the elevated temperature. For further investigating the proton conduction mechanism, the proton conductivities in Arrhenius plot were depicted in Fig. 10, from which the values of activation energy (*Ea*, Table 1) were calculated using Arrhenius equation. Previous study has demonstrated that vehicle mechanism and Grotthuss mechanism co-exist in the proton transfer of CS-based membranes under hydrated condition [45]. Close to the value in literature, CS control membrane had the *Ea* of 10.94 kJ mol^{-1} [34]. By comparison, the *Ea* values of nanohybrid membranes were increased to the range of 11.27–14.62 kJ mol^{-1}. Considering that the *Ea* value for only Grotthuss mechanism was in the range of 14.3–39.8 kJ mol^{-1}, the *Ea* increase suggested that the Grotthuss mechanism tended to be the primary route of proton conduction in nanohybrid membranes. The GO/SGO nanosheets provided additional hoping sites (acid groups and acid–base pairs) to the nanohybrid membrane, which would allow more protons migrate via Grotthuss manner. This finding was in agreement with the conductivity analysis. SGO-filled membrane displayed slightly higher *Ea* value than GO-filled membrane under identical conditions, probably due to the facile hoping sites of acid–base pairs. These results were in good agreement with those found for other types of acid–base composite membranes [46,47].

Table 1
The values of activation energy of CS control and nanohybrid membranes under hydrated and anhydrous conditions.

Membrane	*Ea* under hydrated conditions (kJ mol^{-1})	*Ea* under anhydrous conditions (kJ mol^{-1})
CS	10.94	13.85
CS/GO-0.5	11.27	14.24
CS/GO-1	12.42	15.48
CS/GO-1.5	12.13	14.83
CS/GO-2	11.75	14.81
CS/GO-2.5	11.56	14.43
CS/S2GO-0.5	11.47	15.10
CS/S2GO-1	11.75	15.57
CS/S2GO-1.5	12.26	15.61
CS/S2GO-2	12.80	15.67
CS/S2GO-2.5	12.04	15.38
CS/S4GO-0.5	13.09	14.91
CS/S4GO-1	13.57	15.19
CS/S4GO-1.5	14.35	15.38
CS/S4GO-2	14.62	15.48
CS/S4GO-2.5	13.76	15.10

3.5.3. Proton conductivity of the membranes under anhydrous condition

PEMFC working at elevated temperatures and anhydrous conditions is much more preponderant according to the following advantages: (i) easy water and heat management; (ii) relieving carbon monoxide poisoning of the platinum electrocatalyst; and (iii) accelerating reaction rate at both electrodes [14,46]. However, most of the developed PEMs suffer from conductivity decline under such conditions due to the evaporation of water. Therefore, it is important and impending to develop highly conductive membrane under anhydrous condition. As acid–base pairs possess unique anhydrous proton conduction behaviors through the direct hoping between proton donor (acid group) and acceptor (base group), the conductivities of the as-prepared membranes under 120 °C and anhydrous conditions were measured and the results were shown in Fig. 11a. CS control membrane displayed acceptable anhydrous proton transfer ability with the conductivity of 5.7 mS cm^{-1}. The addition of $-CO_2H$ groups conferred the CS/GO-X higher conductivity than CS control membrane, and CS/GO-1.0 achieved the highest conductivity of 7.9 mS cm^{-1}. By comparison, SGO gave much higher proton conductivities to the nanohybrid membranes, corroborating the effective conducting ability of the acid–base pairs. In addition, the conductivity of SGO-filled membrane could be tailored by the sulfonic acid group loading amount and content of SGO. It should be noted that the proton conductivity under hydrated condition of SGO-filled nanohybrid membrane (up to

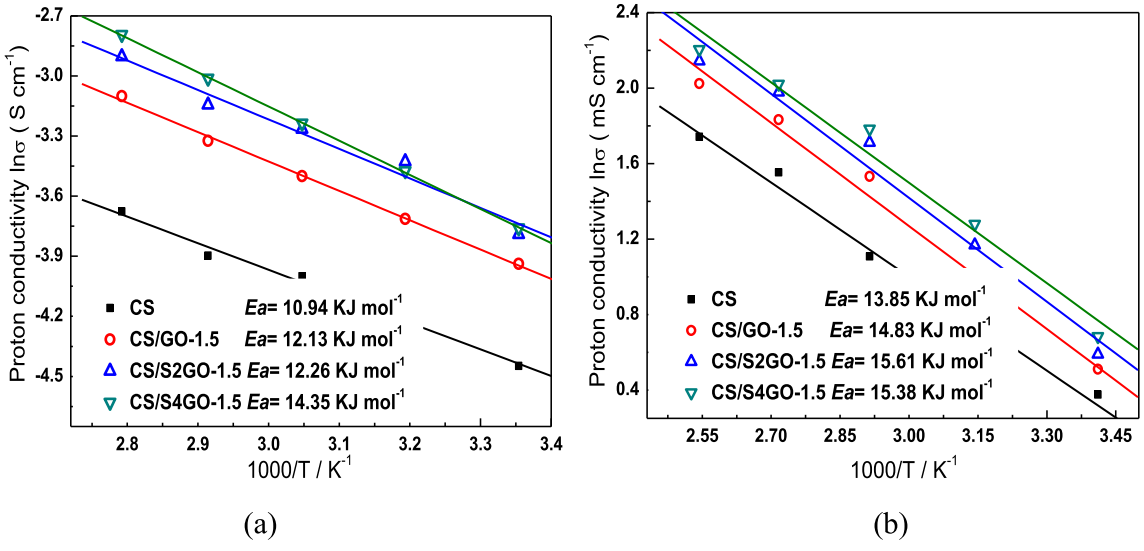

Fig. 10. Arrhenius plots of proton conductivity of CS control and nanohybrid membranes under (a) hydrated condition and (b) anhydrous condition.

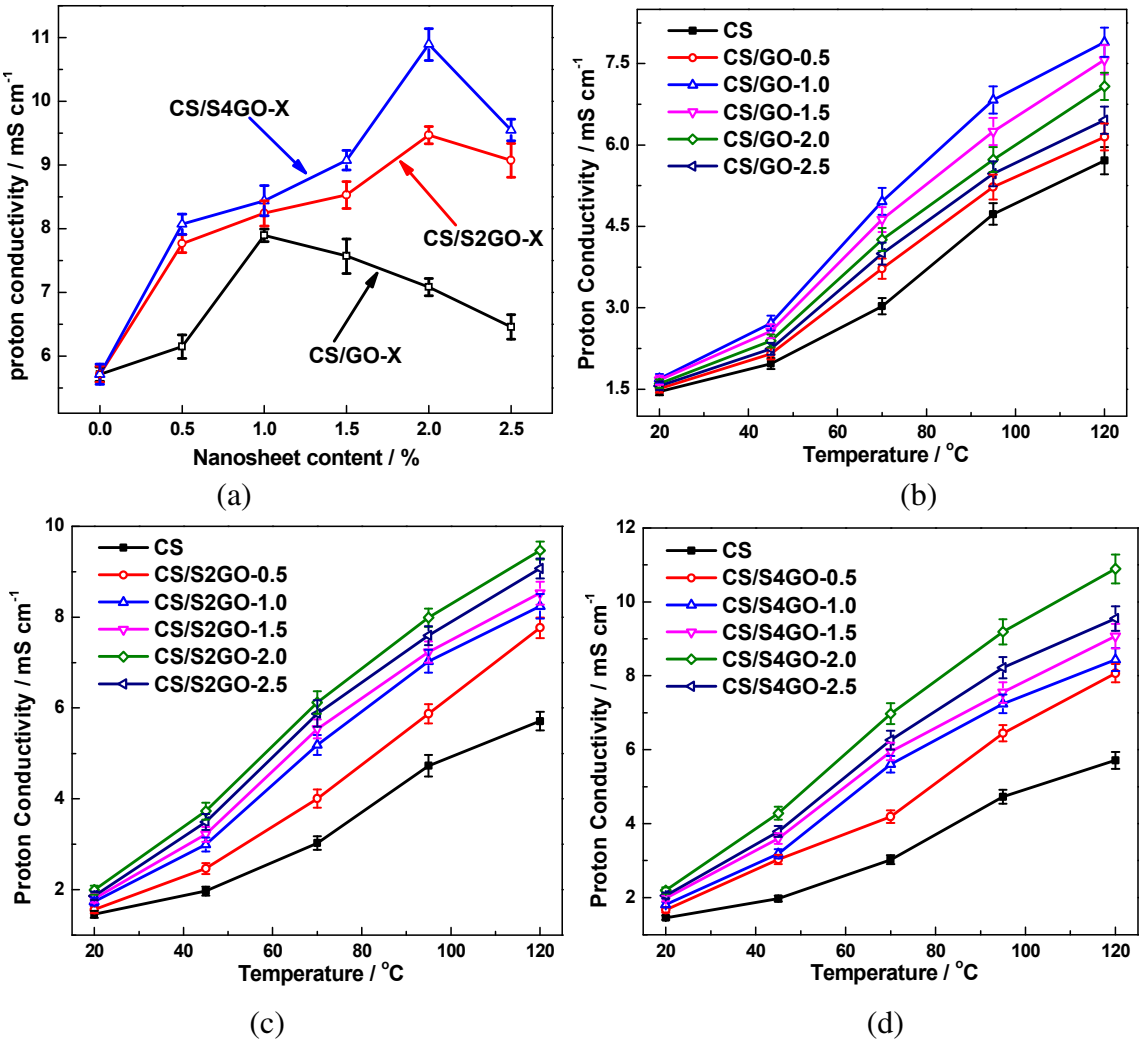

Fig. 11. (a) Proton conductivity at 120 °C and anhydrous condition, and temperature-dependent conductivity of (b) CS/GO-X, (c) CS/S2GO-X, and (d) CS/S4GO-X under anhydrous condition.

0.07 S cm^{-1}) was comparable to that of Nafion (about 0.1 S cm^{-1}) [3]. While under anhydrous condition, the nanohybrid membrane achieved much higher proton conductivity (up to 11.0 mS cm^{-1}) than Nafion (0.1 mS cm^{-1}) [36], inferring the excellent conducting ability of acid–base pairs. The high conductivity might endow the nanohybrid membrane with high PEMFC performances.

The temperature-dependent conductivities under anhydrous condition were depicted in Fig. 11b–d, which suggested that all the membranes showed continuous increase of conductivities with the temperature. The conductivity of CS control membrane increased from 1.5 to 5.7 mS cm^{-1} as the temperature increased from 20 to 120 °C, with the growth rate of 291%. By comparison, more evident enhancements of 366% (from 1.7 to 7.9 mS cm^{-1}), 376% (from 2.0 to 9.5 mS cm^{-1}), and 395% (from 2.20 to 10.9 mS cm^{-1}) were achieved for CS/GO-1.0, CS/S2GO-2.0, and CS/S4GO-2.0, respectively. Such findings indicated that the acid–base pairs at CS–SGO interface could work as facile pathways for proton hoping without water, especially under the elevated temperatures. This feature made the acid–base paired materials more suitable for the application of temperature-sensitive conductors. The *Ea* values for proton condition of the membranes under anhydrous condition were also obtained from the Arrhenius plots (Fig. 11b). Under this condition, the protons mainly transported via Grotthuss mechanism, leading to higher *Ea* values for all the membranes than those under hydrated condition. Similar to the *Ea* tendency under hydrated condition, the nanohybrid membranes had higher *Ea* values than CS control membrane due to the presence of the additional hoping sites, which increased the Grotthuss-type proton transfer.

3.5.4. The stability of proton conductivity

Sufficient stability of proton conductivity of PEM is curial to the stable performances of a fuel cell. Considering the high proton conductivity and structural stability of S4GO-filled membranes, CS/S4GO-2 was chosen as representative to evaluate the conductivity stability under both hydrated and anhydrous conditions. Fig. 12 revealed that the membrane displayed fairly constant proton conductivity under these two conditions over days. Typically, proton conductivity varied from 27.9 to 29.0 mS cm^{-1} with the average value of 28.48 mS cm^{-1} at 30 °C and hydrated conditions, and it changed within the range of 10.7–11.2 mS cm^{-1} with an average value of 10.9 mS cm^{-1} at 120 °C and anhydrous conditions. The stable proton conduction behaviors of CS/S4GO-2 were probably attributed to the covalently grafting of $-SO_3H$ groups on the nanosheets, which provided stable hoping sites and transfer pathways to the nanohybrid membrane. In summary, the above results successfully proved that the SGO nanosheets synthesized in

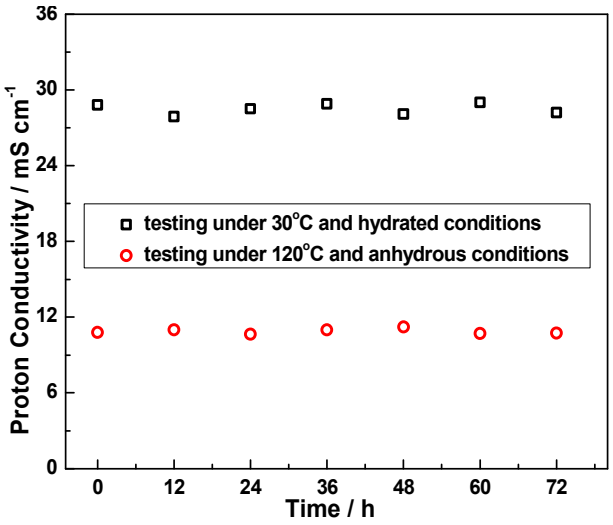

Fig. 12. Time-dependent conductivity of CS/S4GO-2 under 30 °C and hydrated conditions (rectangle) and 120 °C and anhydrous conditions (circle).

this study could significantly enhance the proton transfer ability of basic materials by forming acid–base pairs under both hydrated and anhydrous conditions, especially at the elevated temperature.

3.5.5. PEMFC performances of the membranes

Considering the unique advantages of the elevated-temperature PEMFC and the superior anhydrous conductivity of the nanohybrid membrane, the single cell performances were performed under elevated temperature and anhydrous conditions. Due to the good comprehensive performances of proton conductivity and structural stability, CS/GO-2, CS/S2GO-2, CS/S4GO-2, and CS control membrane were chosen as representatives and then measured under 120 °C and 0% RH. Similar thickness was utilized for each membrane to ensure a good comparison. Fig. 13 revealed that CS control membrane attained the open circuit voltage (OCV) of 0.95 V, inferring a good H_2 barrier ability. Meanwhile, the anhydrous conduction ability afforded the control membrane acceptable cell performances with the maximum current density and power density of about 284.0 mA cm^{-2} and 81.2 mW cm^{-2}, respectively. Compared with the control membrane, the nanohybrid membranes acquired much better cell performances. The OCVs were elevated to 0.97 0.98, and 0.99 V for CS/GO-2, CS/S2GO-2, and CS/S4GO-2, respectively. The increased OCVs indicated that the presence of GO/SGO within CS matrix widened and lengthened the transfer pathways for H_2 molecules, thus enhancing the H_2 resistance abilities of nanohybrid membranes. In addition, it was found that incorporating 2% S2GO could provide a 58% increase of the maximum current density (448.7 mA cm^{-2}) and a 64% increase of the maximum power density (132.9 mW cm^{-2}). The enhanced proton conductivity should be the main factor for the elevated performances, which could reduce the electrolyte resistance of MEAs and facilitated the reduction reaction in cathode [35,48]. For the nanohybrid membranes, the cell performances increased in the order of CS/GO-2 < CS/S2GO-2 < CS/S4GO-2, in accordance with the order of their proton conductivities. This finding supported the fact that proton conductivity of PEM played a critical role in its cell performances. It should be noted that CS/S4GO-2 achieved the highest current density (459.3 mA cm^{-2}) and power density (146.7 mW cm^{-2}), and these data were also higher than those of Nafion under similar conditions [49]. Clearly, these results indicated that the SGO gave obvious enhancement in the cell performances of CS-based PEM. Together with the low cost of CS, the as-prepared nanohybrid membranes might have potential applications for PEMFC.

4. Conclusions

In this study, we reported an attempt for highly conductive nanohybrid membrane by incorporating SGO nanosheets into CS matrix. SGO nanosheets with tunable sulfonic acid group loading amount were synthesized via the facile approach of distillation–precipitation polymerization. The systemic characterizations of the membranes confirmed that the uniformly dispersed SGO improved the thermal and mechanical stabilities of nanohybrid membrane by inhibiting the motion of CS chains through the interfacial attractions. The conductivity measurements proved that SGO donated significant enhancement in proton conductivity to the nanohybrid membranes under both hydrated and anhydrous conditions by means of (i) the generation of acid–base pairs at

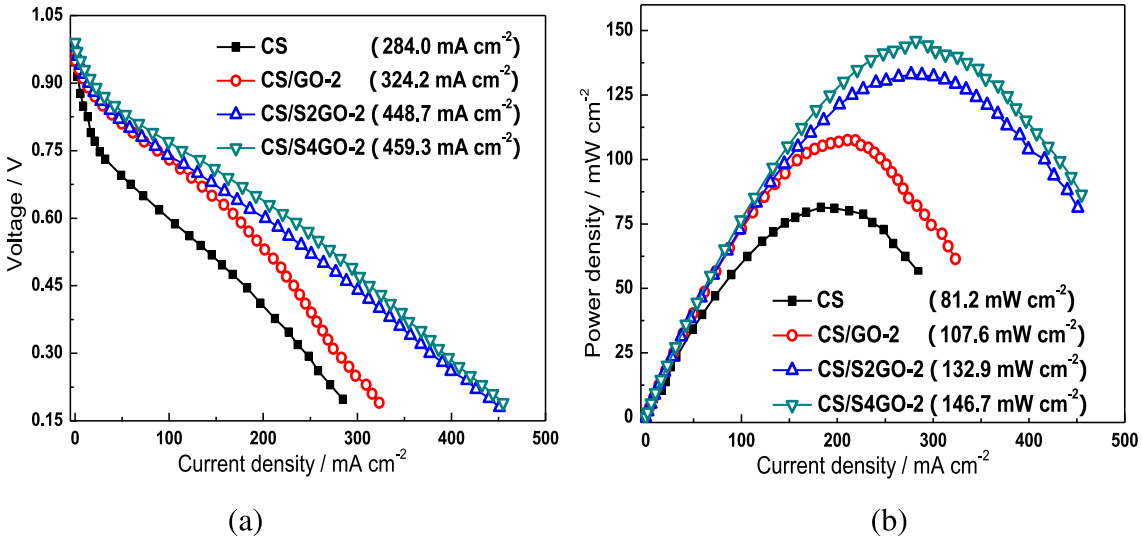

Fig. 13. Single H_2/O_2 cell performances of CS control and nanohybrid membranes under 120 °C and anhydrous conditions: (a) polarization curves and (b) power density–current density curves.

CS–SGO interface, which worked as facile proton-hoping sites, and (ii) the nanosheet structure and high specific surface area of SGO, which allowed the hoping sites form continuous and wide pathways, affording efficient proton migration to the SGO-filled membrane. Moreover, increasing the sulfonic acid group loading amount or content of SGO provided more transfer pathways and thereby further enhanced the proton conductivity. The stable structure of the nanohybrid membrane contributed to stable proton transfer behaviors over days under both hydrated and anhydrous conditions. Benefiting from the enhanced proton conductivity, the nanohybrid membrane achieved much higher H_2/O_2 PEMFC performances than those of the control membrane and Nafion under elevated temperature and anhydrous conditions. Considering the facile preparation process, the present study might provide a potential strategy on the rational design and preparation of highly conductive proton conductors under various conditions.

Acknowledgment

We gratefully acknowledge the financial supports from National Natural Science Foundation of China (21206151 and 21276244), and China Postdoctoral Science Foundation (2012M521409 and 2014T70687).

References

[1] Z. Jiang, Z.-J. Jiang, J. Membr. Sci. 456 (2014) 85–106.
[2] M.M. Hasani-Sadrabadi, E. Dashtimoghadam, N. Mokarramd, F.S. Majedi, K.I. Jacob, Polymer 53 (2012) 2643–2651.
[3] B.G. Choi, Y.S. Huh, Y.C. Park, D.H. Jung, W.H. Hong, H.S. Park, Carbon 50 (2012) 5395–5402.
[4] A.A. Argun, J.N. Ashcraft, P.T. Hammond, Adv. Mater. 20 (2008) 1539–1543.
[5] B.P. Vinayan, R. Nagar, N. Rajalakshmi, S. Ramaprabhu, Adv. Funct. Mater. 22 (2012) 3519–3526.
[6] Z.L. Yao, Z.H. Zhang, L. Wu, T.W. Xu, J. Membr. Sci. 455 (2014) 1–6.
[7] M.A. Hickner, H. Ghassemi, Y.S. Kim, B.R. Einsla, J.E. McGrath, Chem. Rev. 104 (2004) 4587–4612.
[8] P.N. Venkatesan, S. Dharmalingam, J. Membr. Sci. 435 (2013) 92–98.
[9] H. Zhang, C. Ma, J. Wang, X. Wang, H. Bai, J. Liu, Int. J. Hydrogen Energy 39 (2014) 974–986.
[10] H. Liao, K. Zhang, G. Xiao, D. Yan, J. Membr. Sci. 447 (2013) 43–49.
[11] Y. Heo, H. Im, J. Kim, J. Membr. Sci. 425–426 (2013) 11–22.
[12] J. Wang, L. Xiao, Y. Zhao, H. Wu, Z. Jiang, W. Hou, J. Power Sources 192 (2009) 336–343.
[13] K. Suzuki, Y. Iizuka, M. Tanaka, H. Kawakami, J. Mater. Chem. 22 (2012) 23767–23772.
[14] D.W. Shin, N.R. Kang, K.H. Lee, D.H. Cho, J.H. Kim, W.H. Lee, Y.M. Lee, J. Power Sources 262 (2014) 162–168.
[15] R.A.A. Muzzarelli, Carbohydr. Polym. 84 (2011) 54–63.
[16] J.M. Yang, H.C. Chiu, J. Membr. Sci. 419–420 (2012) 65–71.
[17] T. Srinophakun, S. Martkumchan, Carbohydr. Polym. 88 (2012) 194–200.
[18] B. Smitha, S. Sridhar, A.A. Khan, Eur. Polym. J. 41 (2005) 1859–1866.
[19] B.P. Tripathi, V.K. Shahi, Prog. Polym. Sci. 36 (2011) 945–979.
[20] H. Bai, H. Zhang, Y. He, J. Liu, B. Zhang, J. Wang, J. Membr. Sci. 454 (2014) 220–232.
[21] Y. Xiao, Y. Xiang, R. Xiu, S. Lua, Carbohydr. Polym. 98 (2013) 233–240.
[22] H. Wu, W. Hou, J. Wang, L. Xiao, Z. Jiang, J. Power Sources 195 (2010) 4104–4113.
[23] Y. Wan, B. Peppley, K.A.M. Creber, V.T. Bui, E. Halliop, J. Power Sources 162 (2006) 105–113.
[24] S. Yuan, Q. Tang, B. He, H. Chen, Q. Li, C. Ma, S. Jin, Z. Liu, J. Power Sources 249 (2014) 277–284.
[25] Y.S. Choi, T.K. Kim, E.A. Kim, S.H. Joo, C. Pak, Y.H. Lee, H. Chang, D. Seung, Adv. Mater. 20 (2008) 2341–2343.
[26] Z. Jiang, X. Zhao, Y. Fu, A. Manthiram, J. Mater. Chem. 22 (2012) 24862–24869.
[27] D.C. Lee, H.N. Yang, S.H. Park, W.J. Kim, J. Membr. Sci. 452 (2014) 20–28.
[28] Y.-S. Ye, M.-Y. Cheng, X.-L. Xie, J. Rick, Y.-J. Huang, F.-C. Chang, B.-J. Hwang, J. Power Sources 239 (2013) 424–432.
[29] Z. Jiang, X. Zhao, A. Manthiram, Int. J. Hydrogen Energy 38 (2013) 5875–5884.
[30] K. Feng, B. Tang, P. Wu, ACS Appl. Mater. Interfaces 5 (2013) 13042–13049.
[31] Y. He, C. Tong, L. Geng, L. Liu, C. Lü, J. Membr. Sci. 458 (2014) 36–46.
[32] R. Kumar, M. Mamlouk, K. Scott, RSC Adv. 4 (2014) 617–623.
[33] D.C. Marcano, D.V. Kosynkin, J.M. Berlin, A. Sinitskii, Z. Sun, A. Slesarev, L.B. Alemany, W. Lu, J.M. Tour, ACS Nano 4 (2010) 4806–4814.
[34] J. Wang, H. Zhang, X. Yang, S. Jiang, W. Lv, Z. Jiang, S.Z. Qiao, Adv. Funct. Mater. 21 (2011) 971–978.
[35] Y. He, J. Wang, H. Zhang, T. Zhang, B. Zhang, S. Cao, J. Liu, J. Mater. Chem. A 2 (2014) 9548–9558.
[36] J. Zeng, B. He, K. Lamb, R.D. Marco, P.K. Shen, S.P. Jiang, ACS Appl. Mater. Interfaces 5 (2013) 11240–11248.
[37] Ravikumar, K. Scott, Chem. Commun. 48 (2012) 5584–5586.
[38] J. Wang, H. Zhang, Z. Jiang, X. Yang, L. Xiao, J. Power Sources 188 (2009) 64–74.
[39] Y. Wan, K.A.M. Creber, B. Peppley, V.T. Bui, J. Membr. Sci. 280 (2006) 666–674.
[40] T.J. Peckham, S. Holdcroft, Adv. Mater. 22 (2010) 4667–4690.
[41] Y. Wang, D. Yang, X. Zheng, Z. Jiang, J. Li, J. Power Sources 183 (2008) 454–463.
[42] H. Zhang, T. Zhang, J. Wang, F. Pei, Y. He, J. Liu, Fuel Cells 13 (2013) 1155–1165.
[43] L. Vilčiauskas, M.E. Tuckerman, G. Bester, S.J. Paddison, K.-D. Kreuer, J. Nat. Chem. 22 (2012) 461–466.
[44] S.J. Peighambardoust, S. Rowshanzamir, M. Amjadi, Int. J. Hydrogen Energy 35 (2010) 9349–9384.
[45] J.R. Salgado, Electrochim. Acta 52 (2007) 3766–3778.
[46] M. Yamada, I. Honma, J. Phys. Chem. B 108 (2004) 5522–5526.
[47] H. Pu, D. Wang, Electrochim. Acta 51 (2006) 5612–5617.
[48] X. Zhang, Z. Hu, Y. Pu, S. Chen, J. Ling, H. Bi, S. Chen, L. Wang, K. Okamoto, J. Power Sources 216 (2012) 261–268.
[49] M.S. Kang, M.J. Lee, Electrochem. Commun. 11 (2009) 457–460.